EurJIC
European Journal of Inorganic Chemistry

Full Paper
doi.org/10.1002/ejic.202000423

Chemistry Europe
European Chemical Societies Publishing

Copper(I) Dimers

Synthesis, Crystal Structure, and DFT Study of Two New Dinuclear Copper(I) Complexes Bearing Ar-BIAN Ligands Functionalized with NO_2 Groups

Mani Outis,[a] Vitor Rosa,*[a] César A. T. Laia,[a] João Carlos Lima,[a] Sónia Barroso,[b][‡] Ana Luísa Carvalho,[b] Maria José Calhorda,*[c] and Teresa Avilés*[a]

Dedicated to Jean-François Halet on the occasion of his 60th birthday

Abstract: Two new bis(aryl-imino)-acenaphthene, Ar-BIAN (Ar = 2,4,6-trimethylphenyl = mes) ligands, bearing the NO_2 group in the naphthalene moiety of the iminoacenaphthene at *para*- (5-NO_2) and *meta*- (4-NO_2) position, of formulations 1,2-bis(mes-imino)-5-nitroacenaphthene, **1**, and 1,2-bis(mes-imino)-4-nitroacenaphthene, **2**, were synthesized. Their respective dinuclear iodide bridged copper(I) complexes $[Cu_2(\mu\text{-}I)_2(\text{mes-BIAN-5-}NO_2)_2]$, **3** and $[Cu_2(\mu\text{-}I)_2(\text{mes-BIAN-4-}NO_2)_2]$, **4**, were obtained in good yields by treatment with an equimolar amount of CuI. All compounds were characterized by elemental analysis, single-crystal X-ray diffraction, ^{1}H-NMR, ^{13}C-NMR, FTIR, UV/Vis spectroscopy. DFT calculations helped to understand the different molecular structure observed in the crystals of **3** and **4** and the determining role of packing forces. TDDFT revealed that the absorption bands in the visible were essentially MLCT (Metal to Ligand Charge Transfer), with some n→π* character (intra ligand). The shift to the red compared to the spectrum of the Cu(I) complex analogue without the NO_2 group, $[Cu_2(\mu\text{-}I)_2](\text{mes-BIAN})_2]$, **6**, could be explained by the stabilization of the ligand unoccupied π* orbitals in the presence of NO_2.

Introduction

The design and synthesis of copper complexes is a subject of current interest since they can be applied in a large variety of metal-mediated transformations.[1] Moreover, copper is a cheap, abundant and non-toxic metal. d^{10} transition metal complexes have been extensively studied because of their unique photophysical and photochemical properties which led to applications for light emitting devices, sensing devices, solar cells, and artificial photosynthesis.[2] Among those, $3d^{10}$ copper(I) complexes were studied since the last century to explore their photophysical properties.[3]

The well-known $\{Cu_2(\mu\text{-}X)_2\}$ core (X = halide) can coordinate to different types of ligands to form a wide variety of complexes, resulting in tetracoordination around the Cu(I) atom. Their general formulation is $[Cu_2(\mu\text{-}X)_2L_4]$, in which L are mainly N or P ligands, either monodentate (L), or bidentate chelating ligands (L-L).[4] The synthesis and photophysical properties of Cu(I) compounds of this type, bearing chelating chiral bis(phosphines), has been reported.[5]

α-Diimine ligands are well known and have been extensively used due to their ability to stabilize organometallic complexes.[6,7] Elsevier et al.[8] described the synthesis and full characterization of a new family of rigid chelating bidentate ligands of the type Ar-BIAN (bis(aryl)acenaphthenequinonediimine) by condensation of acenaphthenequinone with two equivalents of an appropriate aryl-amine. Many late transition metal complexes bearing α-diimine ligands have been extensively employed in several catalytic reactions.[9–16] Using this synthetic route, we can easily vary the backbone and the aryl substituents, enabling thus to tune the steric and electronic effects at the metal centre. We have been engaged during the last decade in the synthesis of α-diimine transition metal compounds, either for structural studies[17–21] or catalytic applications.[22–27] Furthermore, copper(I) complexes bearing Ar-BIAN ligands have been reported by us[18,22–24,26] and other authors.[28]

The excellent redox properties, stereo and electronic tunability of the bis(aryl)acenaphthenequinonediimine (Ar-BIAN) li-

[a] *M. Outis, Dr. V. Rosa, Prof. Dr. C. A. T. Laia, Prof. Dr. J. C. Lima, Prof. Dr. T. Avilés*
LAQV, REQUIMTE, Departamento de Química, Faculdade de Ciências e Tecnologia, Universidade Nova de Lisboa,
2829–516 Caparica, Portugal
E-mail: teresa.aviles@fct.unl.pt
vitor.rosa@fct.unl.pt
mjc@fc.ul.pt
https://laqv.requimte.pt/people/41-maria_teresa_aviles_perea
[b] *Dr. S. Barroso, Dr. A. L. Carvalho*
UCIBIO, REQUIMTE, Departamento de Química, Faculdade de Ciências e Tecnologia, Universidade Nova de Lisboa,
2829–516 Caparica, Portugal
[c] *Prof. Dr. M. J. Calhorda*
BioISI - Biosystems & Integrative Sciences Institute, Departamento de Química e Bioquímica, Faculdade de Ciências, Universidade de Lisboa,
1749–016 Lisboa, Portugal
[‡] Current address: MARE – Centro de Ciências do Mar e do Ambiente, Politécnico de Leiria,
2520–641 Peniche, Portugal
Supporting information and ORCID(s) from the author(s) for this article are available on the WWW under https://doi.org/10.1002/ejic.202000423.

gands, make them extremely useful in the contexts of synthetic, structural, and catalytic chemistry, their photophysical properties have been studied and are found in the literature.[29–34]

Cu(I)–BIAN complexes have been studied as photosensitizers, for potential photovoltaic applications[35,36] and as photocatalysts.[37]

We are interested in the synthesis of new Ar-BIAN ligands and their respective binuclear $\{Cu_2(\mu\text{-}I)_2\}(LL)_2$ complexes, focusing on their full characterization by extensive experimental methods supported by in-depth theoretical calculations. These studies allowed us to determine their structural and electronic properties which could enlighten their potential application as, for example, light harvesters for Dye-Sensitized Solar Cells (DSSC)[36] or as NIR emissive complexes.[30]

Here we report the synthesis, structural characterization and DFT studies of two novel Ar-BIAN ligands bis(mes-imino-5-nitroacenaphthene), **1**, and bis(mes-imino-4-nitroacenaphthene), **2** and their two new dimeric Cu(I) complexes **3** and **4** with a $\{Cu_2(\mu\text{-}I)_2\}$ core, which display a redshifted MLCT, characterized by TDDFT calculations, in comparison with the analogous complex **6** bearing the unsubstituted bis(mes-imino-acenaphthene) ligand.[26]

Results and Discussion

Chemical Studies

The first step in the synthesis of the ligands is the functionalization of acenaphthenequinone by the NO_2 group, which has been described in the literature under different experimental conditions, at room temperature, 0 °C and 80 °C, using $NaNO_3$ or HNO_3 as nitration agents.[38,39] Although the authors claimed that the nitro-acenaphthenequinone held the NO_2 group at the *para*-position, our attempts to repeat the synthesis following the three described methods afforded in all cases a mixture of products functionalized at *para*- and *meta*-position in roughly 1:2 *meta*-:*para*-proportion, from now on we will indistinctly name *para*-position to 5-NO_2 and *meta*-position to 4-NO_2 (Scheme 1).

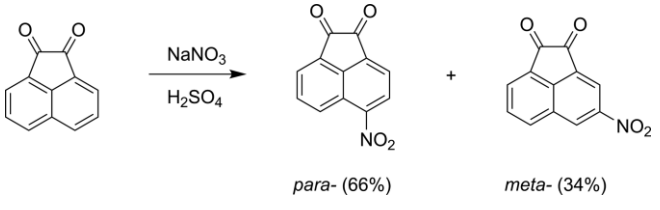

Scheme 1. Nitration of acenaphthenequinone.

The second step is diimine formation, and there are two major synthetic strategies to obtain Ar-BIANs: (i) the template method using $ZnCl_2$ or (ii) using an organic acid as a catalyst. The second method using EtOH as solvent and formic acid as catalyst revealed to be quite efficient since it allowed us to separate the two isomers due to their different solubilities. The two separated Ar-BIANs (Scheme 2), one with the NO_2 group at the *para*-position, **1,** which precipitates from ethanol in 83 % yield, and another with the NO_2 group at the *meta*-position, **2,** remains dissolved in ethanol from which the ligand is isolated after workup in 78 % yield.

Formation of ligands can be confirmed by FTIR spectroscopy. No C=O stretching vibrations of the starting diketones, in the 1700–1800 cm^{-1} region, are observed, discarding thus the formation of monosubstituted species. Characteristic vibrations of NO_2 group are observed for free ligands in the range of 1524–1536 cm^{-1} for symmetric stretching and in the range of 1329–1338 cm^{-1} for the asymmetric stretching of N–O bond. The C=N stretching frequency in the free ligands cannot be assigned unambiguously because of the presence of C=C stretching frequencies from the naphthalene backbone in this region,[8,40] however it is reported in the literature[41] that two bands in the range of 1617–1675 cm^{-1} can be assigned to C=N stretching of Ar-BIANs.

Both ligands **1** and **2** are asymmetric molecules regarding the functionalized naphthalene moiety, ^{1}H-NMR characterization of ligands **1** and **2** was performed in $CDCl_3$. The main differences between the two compounds are in the naphthalene moiety bearing the NO_2 substituent. In the case of ligand **1**, with the *para*-NO_2, we observe two doublets, for protons at the position 3 and 4 at 6.83 and 8.31 ppm, respectively. As for ligand **2**, with the *meta*-NO_2, two singlets corresponding to protons at 3 and 5 positions, were observed with a chemical shift of 7.39 ppm and 8.86 ppm, respectively.

When we look at the protons of the aryl moieties of both compounds, we observe that in the case of ligand **1** they are not strongly affected by the presence of the NO_2 group. Just one singlet, integrating for four protons, at 6.99 ppm, was observed, similar to the unsubstituted ligand **5**. In the case of compound **2**, we see that the protons of the aryl group spatially closer to the NO_2 substituent, undergo some influence from the nitro group. Two singlets, both integrating for two protons at 7.04 ppm and 6.99 ppm were observed. For ligand **2**, the two *para*-methyl groups are not equivalent, contrary to ligands **1** and **5**, showing a clear influence of the *meta*-NO_2 group.

Indications of the presence of possible (E,Z) isomers were found in the ^{1}H-NMR spectra. In order to confirm their presence,

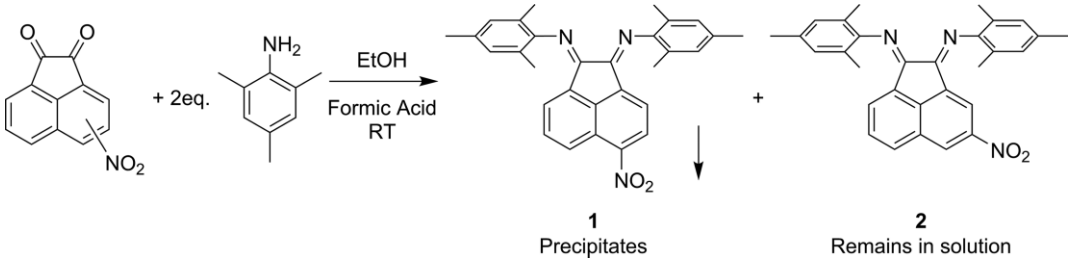

Scheme 2. Synthesis of ligands **1** and **2**.

Full Paper
doi.org/10.1002/ejic.202000423

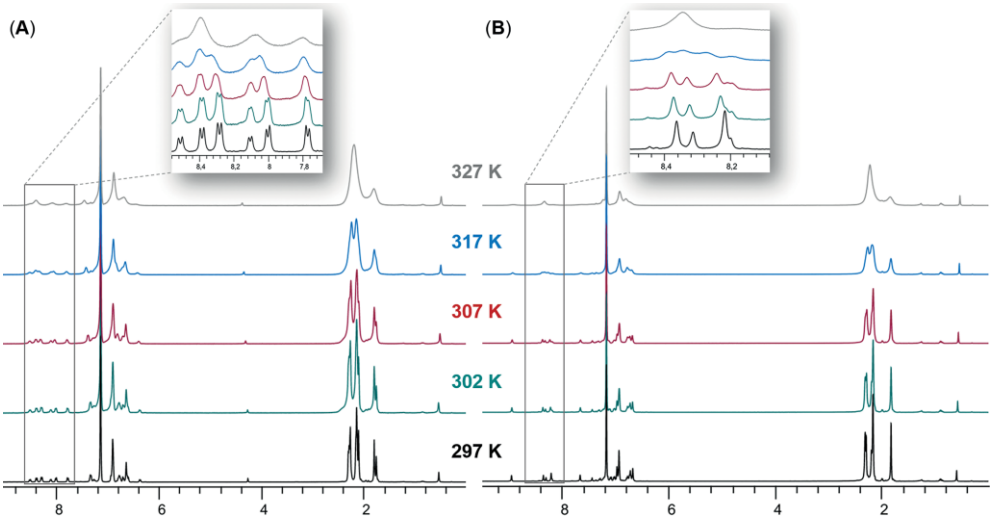

Figure 1. Temperature variation study by ^{1}H-NMR spectroscopy in C_6D_6 of ligands **1** (A) and **2** (B). Bottom to top spectra: temperature raise from 297 K to 327 K.

we performed variable temperature ^{1}H-NMR experiments in C_6D_6.

In solution, the Ar-BIAN ligands may appear in two (E,E) and (Z,E) stereo isomeric forms, since steric repulsion prevents (Z,Z) from existing. Ragaini et al.[42] show that the ratio of the two isomers depends on both temperature and solvent, the complete assignment of signals being possible to make by bidimensional NMR experiments (COSY, NOESY, Figures S1–S10 in Supporting Information, SI). While asymmetric Ar-BIAN (Ar,Ar'-BIAN) molecules appear in both forms in solution, symmetric ones seem to occur only as the (E,E) isomer. **1** and **2**, despite holding the same Ar (2,4,6-trimethylphenyl), are asymmetrical molecules regarding the functionalized naphthalene moiety, so they can exist as (E,E), (Z,E) and (E,Z) forms in solution (see computational studies). While the presence of the isomers is not visible in $CDCl_3$, when the solvent was changed to C_6D_6, (Figures S11 and S12 in SI) all three isomers could be observed, particularly in the case of **1** (S11 in SI). At room temperature in C_6D_6 the three isomers coexist, while at higher temperatures the isomers rapidly change and converge to one set of peaks (see Figure 1).

Complexes **3** and **4** were synthesized using the same strategy adopted for complex $[Cu_2(\mu\text{-}I)_2(Mes\text{-}BIAN)_2]$ **6**,[25] (see Scheme 3), by adding CuI to the stoichiometric amount of ligand **1** or **2** in CH_3CN and refluxing the mixture for 3 h. After removal of the solvent under vacuum, dark solids were isolated, washed with pentane and dried under vacuum. Suitable crystals for single-crystal X-ray structure determination were obtained by slow diffusion of pentane in a CH_2Cl_2 solution, yielding compound **3** and **4** in 66 % and 59 % respectively.

Two different isomers can be formed. In one of them, the ligands are in *trans* conformation (isomer A) and in the other one the ligands are in *cis* conformation (isomer B) (see Scheme 3). In the synthesis of the Cu(I) dimers with ligands **1** and **2**, only isomer A could be isolated as revealed by single-crystal X-ray diffraction (see below).

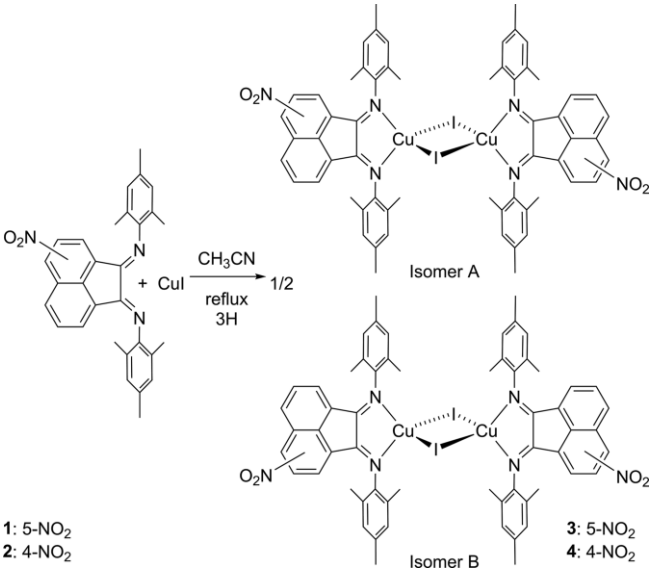

Scheme 3. Synthesis of complexes **3** and **4**, and possible isomers A and B.

Characteristic vibrations of the NO_2 group are observed for complexes **3** and **4** at 1530 and 1536 cm^{-1}, respectively, for symmetric stretching, and for the asymmetric stretching of N–O bond at 1331 and 1339 cm^{-1}, respectively. A band at 1643 cm^{-1} for complex **3** and two bands, at 1649 and 1647 cm^{-1} for complex **4**, can be assigned to C=N stretching.

^{1}H-NMR and ^{13}C-NMR studies of complexes **3** and **4** show similar patterns to those of the ligands, only differing on the chemical shifts (Figures S13–S24 in SI). The highest difference is for the methyl groups in the *ortho*-position of the aryl moieties, that are high field shifted in comparison to the free ligands, at 2.15 ppm for **3**, 2.15 and 2.17 ppm for **4**. For complex **4**, not only the two *para*-methyl groups of the aryl are nonequivalent, like in ligand **2**, but we also observe two peaks assigned to the four *ortho*-methyl groups by opposition to only one peak in

Full Paper
doi.org/10.1002/ejic.202000423

complexes **3** and **6**. The *para*-methyl groups appear as two singlets, at 2.44 and 2.36 ppm, and the four *ortho*-methyl groups appear as two singlets at 2.17 and 2.15 ppm.

Crystallography

Crystals of **1–4** suitable for single-crystal X-ray diffraction were obtained as described in the synthetic procedures. Ligands **1** and **2** crystallize in the monoclinic system, space groups $P2_1/n$ and $C2/c$, respectively. The molecular structures of **1** and **2** are depicted in Figure 2 and selected structural parameters are listed in Table S1 (SI). Structural parameters of the non-substituted 2,4,6-$Me_3C_6H_2$-BIAN analogue, **5**, reported in the literature,[41] are also presented in Table S1 for comparison. The molecular structures of **1** and **2** show that the bis(imino) fragment exhibits the (Z,E)-configuration as some other Ar-BIAN compounds,[18,43] instead of the more common (E,E)-configuration.[44–47] Compound **1**, with a nitro substituent in the *para*-position, presents a more planar bis(imino)acenaphthene skeleton than the non-substituted 2,4,6-$Me_3C_6H_2$-BIAN, **5**, as evidenced by the N(1)–C(29)–C(19)–N(2) and C(28)–C(29)–C(19)–C(20) torsion angles (0.2(7)° and 0.5(4)° in **1** vs. –6.2(2)° and –4.3(2)° in 2,4,6-$Me_3C_6H_2$-BIAN, **5**. In contrast, compound **2**, with a nitro substituent in the *meta*-position, displays a larger deviation from planarity in the bis(imino)acenaphthene moiety than the non-substituted analogue **5**, (N(1)–C(29)–C(19)–N(2) and C(28)–C(29)–C(19)–C(20) torsion angles = 19.1(4)° and 10.2(2)° in **2** vs. –6.2(2)° and –4.3(2)° in **5**). The position of the nitro substituent in the naphthenic rings seems to influence the referred deviation from planarity, possibly due to C–H···O and C–H···π weak hydrogen bonds, as observed in the packing diagram (Figure S25, SI). The angle between the two mesityl rings is about 78° in compound **1** and 92° in compound **2**. The imine C=N bonds N(1)–C(29) in **1** and N(2)–C(19) in **2** are longer than the corresponding bond lengths in 2,4,6-$Me_3C_6H_2$-BIAN, **5**, (1.280(5) Å and 1.276(3) Å vs. 1.2662(16) Å), but overall they are comparable with those observed in other Ar-BIAN compounds.[4–7,47] The breaking of symmetry of the NO_2 substituents seems to disfavour the (E,E) configuration observed when there is symmetry.

The molecular structures of **3** and **4** are depicted in Figure 3 and Figure 4, respectively, and selected structural parameters are listed in Table S2 (SI). Structural parameters of the related {CuI(Ar-BIAN)}$_2$, **6**, with non-substituted 2,4,6-$Me_3C_6H_2$-BIAN ligand, **5** (Figure S26 in SI),[26] previously reported by us, are also presented in Table S2 (SI) for comparison. Compound **3** crystallizes in the monoclinic system, space group $C2/c$, with one half molecule of **3** and one co-crystallized molecule of CH_2Cl_2 in the asymmetric unit. Compound **4** crystallizes in the monoclinic system, space group $P2_1/n$, with one molecule in the asymmetric unit. In both structures the Cu(I) atoms are bridged by two iodide ions and coordinated by two imine nitrogen atoms of the BIAN ligands presenting distorted tetrahedral geometry. The I–Cu–I angles in compound **4** are wider (about 115°) than in compound **3** (106.7(1)°). As a result, the Cu···Cu distance is particularly shorter in compound **4** (2.651(1) Å vs. 3.070(1) Å in **3**) and it is also shorter than the sum of the van der Waals

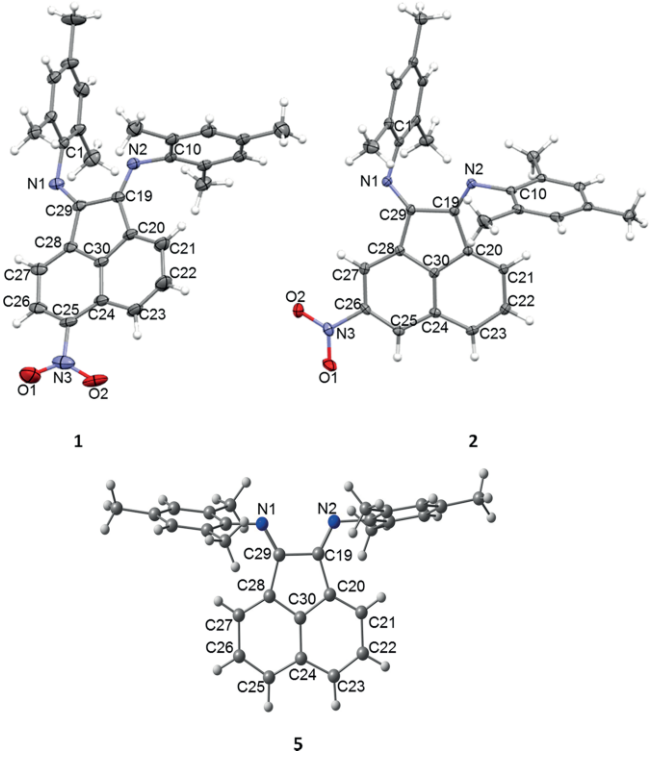

Figure 2. Molecular structures of **1** (top left) and **2** (top right) using 30 % probability level ellipsoids, and molecular structure of 2,4,6-$Me_3C_6H_2$-BIAN, **5**.

radii of two copper atoms (2.80 Å) suggesting a "cuprophilic" interaction in compound **4**.[29,48] Another difference between compounds **3** and **4** is that the CuI dimer is perfectly planar in **3** while in **4** it displays a butterfly conformation with an angle of 160.9(2)° between the triangles formed by Cu(1)–I(1)–Cu(2) and Cu(1)–I(2)–Cu(2) (Figure 4). This distortion of the Cu–$(I)_2$-Cu core has been reported in the literature for other dimeric Cu compounds and it has been related mainly to packing forces.[49,50] The structural differences between compounds **3** and **4** may be either due to steric constraints caused by the nitro *meta*-substituent or to packing arrangement. The packing diagram of **4** shows that all the molecules are arranged in the same direction, with the naphthalene moieties lying on parallel planes (Figure S27, SI, right). For compound **3**, the crystal presents molecules packed perpendicularly to each other (Figure S27, SI, left) similar to the packing arrangement observed for the analogue compound **6** (with non-substituted ligand) {CuI(Ar-BIAN)}$_2$.[26] In fact, the latter compound presents two crystallographically different molecules in the asymmetric unit (molecules ***a*** and ***b*** in Figure S26, SI) whose structural differences may only be attributed to packing forces. In the case of compound **3**, there are no structural differences between the molecules despite the perpendicular arrangement. Interestingly, the structural parameters of **3** are very similar to those of molecule ***a*** of {CuI(Ar-BIAN)}$_2$ (Figure S26, SI) while the structural parameters of **4** are very similar to those of molecule ***b*** of {CuI(Ar-BIAN)}$_2$ (Figure S26, SI) as can be seen in Table S2 (SI). In light of the discussion above, it is plausible to attribute the structural differences between compounds **3** and **4** to packing forces rather than to steric constraints caused by the position

Full Paper
doi.org/10.1002/ejic.202000423

of the nitro substituent. For both compounds the main short contact interactions observed are non-classical C–H···O and C–H···π weak hydrogen bonds, as well as C–H···I halogen bonds connecting the molecules of **3** and **4** in different ways (Figure S27, SI).

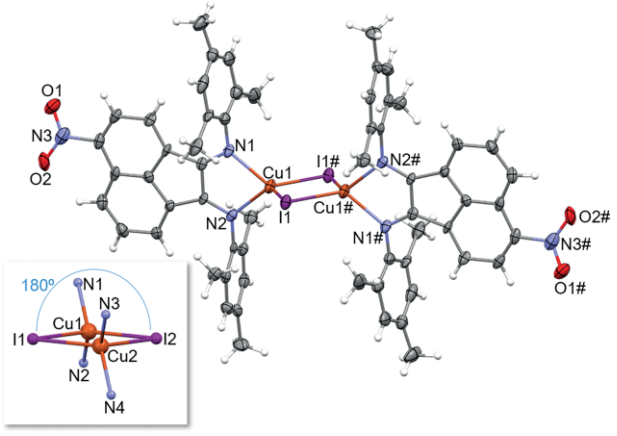

Figure 3. Molecular structure of **3**, using 30 % probability level ellipsoids. Equivalent atoms # are generated using the symmetry transformation –x + 1/2, –y + 1/2, –z + 2. The inset shows the planarity of the Cu–$(I)_2$-Cu core. Selected bond lengths [Å]: I(1)–Cu(1) 2.569(1), I(2)–Cu(1) 2.574(1), Cu(1)–N(1) 2.110(7), Cu(1)–N(2) 2.140(7), Cu(1)···Cu(2) 3.070(1).

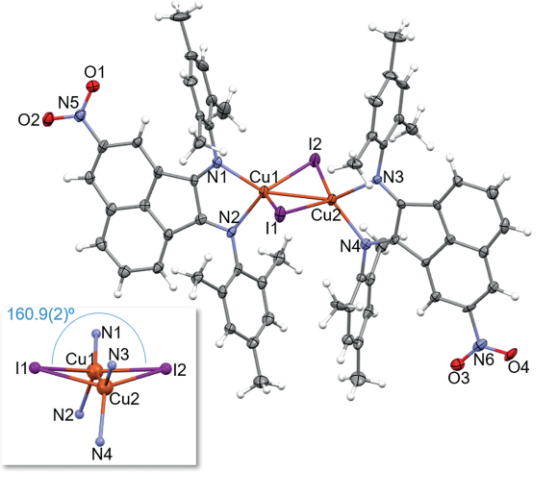

Figure 4. Molecular structure of **4**, using 30 % probability level ellipsoids. The inset shows the butterfly conformation of the Cu–$(I)_2$-Cu core. Selected bond lengths [Å]: I(1)–Cu(1) 2.555(1), I(2)–Cu(1) 2.579(1), Cu(1)–N(1) 2.086(5), Cu(1)–N(2) 2.113(6), I(2)–Cu(2) 2.563(1), I(1)–Cu(2) 2.582(1), Cu(2)–N(3) 2.121(5), Cu(2)–N(4) 2.094(5), Cu(1)···Cu(2) 2.651(1).

Comparing the structural data of compounds **3** and **4** with those of the free ligands **1** and **2**, a slight elongation is observed on the N=C bonds (mean 1.275(11) Å in **3** and 1.281(8) Å in **4**) ascribed to the coordination to the metal. In addition, there is a slight deviation from planarity in the bis(imino)acenaphthene skeleton upon coordination in **3** (N(1)–C(29)–C(19)–N(2) and C(28)–C(29)–C(19)–C(20) torsion angles = 0.2(12)° and –2.0(9)° vs. 0.2(7)° and 0.5(4)° in the free ligand) while in **4** that moiety becomes more planar than in the free ligand (N(1)–C(29)–C(19)–N(2) and C(28)–C(29)–C(19)–C(20) torsion angles = –8.6(9)° and –3.5(6)° vs. 19.1(4)° and 10.2(2)° in the free ligand). The Cu–N and Cu–I bond lengths are in agreement with those observed in the two related {CuI(Ar-BIAN)}$_2$ compounds found in the literature.[26,28]

Computational Studies

The geometries of the ligands and the complexes were optimized using DFT calculations as implemented in Gaussian16,[51] with the PBE1PBE functional, a 6-31G** basis set for the light atoms, and LANL2DZ with polarization for I and Cu, considering the solvent (chloroform) effect and dispersion corrections (more details in Experimental).

The ligand **5** without substituents may adopt two conformations, (E,E) and (Z,E). The (E,E) is slightly more stable (ΔG = 0.6 kcal mol^{-1}). When nitro substituents are introduced, there is another conformation, (E,Z). The three are shown, with the more relevant distances and relative energies, in Figure S28, SI. The two ligands have similar energies, the lowest energy form of **2** (E,E) being ca. 2.4 kcal mol^{-1} more stable than the lowest energy form of **1** (E,Z). The most stable conformation is different for the two ligands. When they bind to a metal, they must rearrange to the (E,E) conformation.

The optimization of the geometry of complexes **3** and **4** was more difficult and it required taking into account dispersion corrections in order to improve the agreement of the geometry of the {$Cu_2(\mu\text{-}I)_2$} core with the experimental one, since M–M interactions in d^{10}-d^{10} systems are difficult to reproduce.

The optimized geometry of **3** is shown in Figure 5 (top) with relevant distances (values are only given for non-equivalent bonds). The {$Cu_2(\mu\text{-}I)_2$} core is planar and the Cu–I and Cu–N

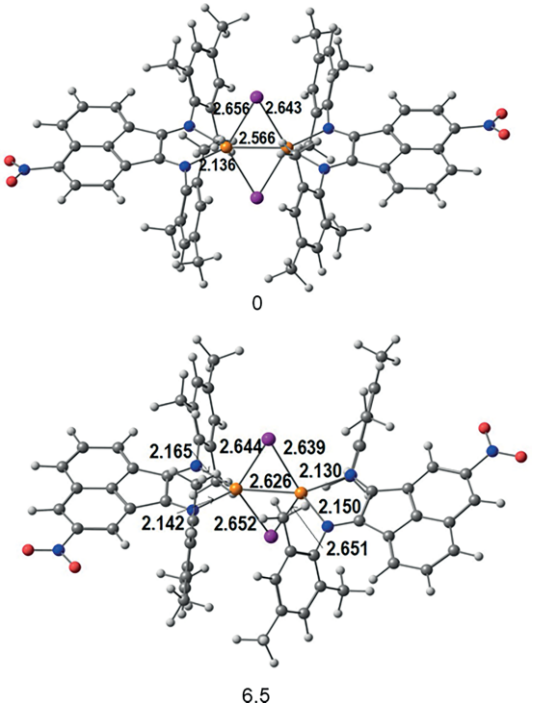

Figure 5. Optimized geometries (isomers A of Scheme 3) of **3** (top) and **4** (bottom) showing some bond lengths [Å] and relative energies (ΔG, kcal mol^{-1}).

Full Paper
doi.org/10.1002/ejic.202000423

bonds are very similar to the experimental ones (Table S2), the only significant difference being observed in the Cu–Cu distance, calculated as 2.566 Å, but determined as 3.071 Å. To check this aspect, the Cu–Cu distance of the $\{Cu_2(\mu\text{-}I)_2\}$ in the core of the complex **3**, was varied from 2.566 Å to 3.071 Å in several steps and the energy increased by 2.9 kcal mol^{-1} (electronic energies, see also below). Considering the size of the molecule and the small energy difference (very flat potential energy surface), it might be possible, but resources consuming, to modify the methodology to get a better agreement.

The optimized geometry of complex **4** (Figure 5, bottom) is very similar to the experimentally determined. Even the Cu–Cu distance is very close, and the I-CuCu$_{med}$–I butterfly angle was calculated as 166.1° (experimental 166.8°). CuCu$_{med}$ is the point in the centre of the line joining the copper atoms. Complex **4**, with NO_2 in the *meta*-position, is more stable (6.5 kcal mol^{-1}) than complex **3** with this group in *para*- position, following the order of stability of the ligands.

The two complexes exhibit different $\{Cu_2(\mu\text{-}I)_2\}$ cores, namely flat with a long Cu–Cu distance as seen in **3** and puckered with a Cu–Cu bond **4**. Also, the phenyl groups of the two Ar-BIAN ligands are parallel in **3** (Figure 3) and are not parallel in **4** (Figure 4). One should be tempted to assign the preference to the substitution pattern, since the NO_2 group occupies *para* and *meta* positions in **3** and **4**, respectively. It is not that simple because the analogous complex without substituent, **6**, has been structurally characterized and both forms are also present. When the geometry is optimized, starting from any of them, the energy minimum corresponds to the flat $\{Cu_2(\mu\text{-}I)_2\}$ core, though the Cu–Cu distance is too short as seen above for **3**. Other distances are very comparable to those in **3** and **4**. Since there are no substituents, the origin must be found elsewhere. A closer look at the two independent molecules present in the crystal structure of **6**, emphasizing the position they occupy (Figure 6), shows on the left the flat core (Cu–Cu distance 3.08 Å) with parallel phenyl rings, while the unit on the right is puckered with a Cu–Cu bond and not parallel phenyl groups (not so easily seen in this view). Also, the BIAN moiety of the right-hand side unit is sandwiched between two of the phenyl groups of the left unit. In order to maximize the interaction, the arrangement must be planar. The packing forces the geometry to adapt, distorting the $\{Cu_2(\mu\text{-}I)_2\}$ core, which requires a small amount of electronic energy (2.9 kcal mol^{-1}, see Figure S29 in SI), compensated by intermolecular interactions. The packing arrangement of **3** and **4** is probably responsible for the molecular structures observed. Indeed, in complex **3** a very similar π–π stacking with three aryl rings is observed, reinforcing the previous interpretation.

A related question is prompted by the representation of a Cu–Cu bond in the crystal structure of **4**, but not in the structure of **3** (Figure 3 and Figure 4). In complexes **3**, **4**, and **6**, iodine atoms bridge the copper ones. As distances are not reliable indicators to detect bonds, we calculated Wiberg indices (see Computational studies), which scale as bond strength indicators. For calibration a structure with a non-supported Cu(I)–Cu(I) was searched in the CSD[52] (see molecular representation in Figure S30, SI). The Wiberg index (WI) is 0.189 for the experimental structure and 0.190 for the structure optimized in the same conditions as the other complexes. The optimized structures of **3**, and **6** led to WI of 0.193, and **4** to 0.178. This would indicate a bond as strong as the reference non-supported Cu(I)–Cu(I). However, as the experimental geometries could not be exactly reproduced as discussed above, we calculated WIs for them. Now, the WI for **6** is 0.090 (a) and 0.148 (b), for **3** 0.09, and for **4** 0.132. The distortion produced by packing effects weakens the Cu–Cu bonds, less in **3** and **6a** (ca. 75 %) and more in **4** and **6b** (ca. 50 %). Probably there is a Cu–Cu in all the complexes, though weaker in **4** and **6b**.

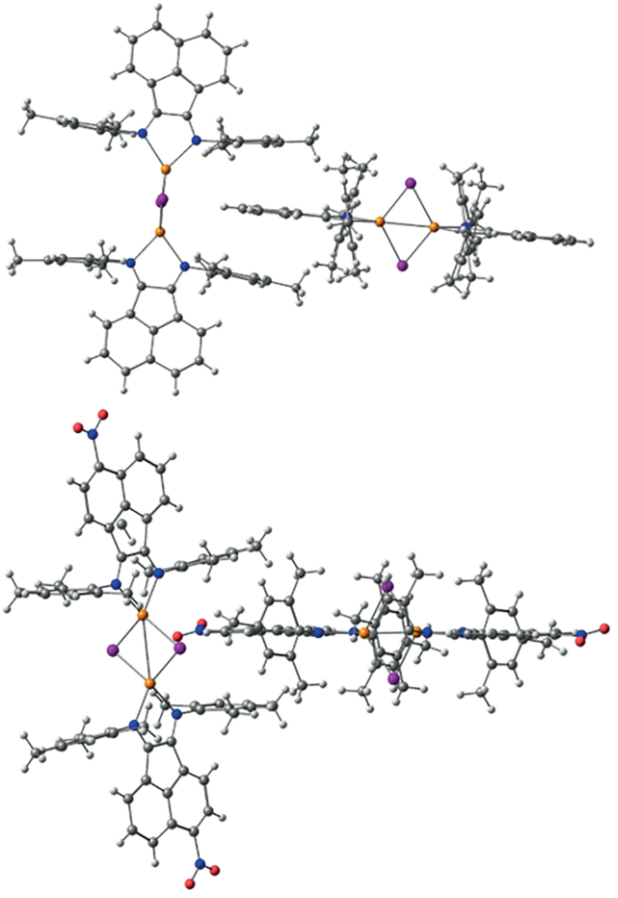

Figure 6. Molecular structure of $\{CuI(Ar\text{-}BIAN)\}_2$ (**6**), showing the two crystallographically different molecules present packed in the asymmetric unit (top) and of **3** showing the same type of motif built from identical units (bottom).

Absorption Spectra

Ligands and complexes absorb in the visible and UV regions, but the complexation leads to a shift of the lower energy bands to longer wavelengths, especially when the NO_2 substituents are present, as shown in Figure 7 and Table S3 (SI). (See also Figure S31 in SI for comparison purposes).

TDDFT calculations were used to obtain the absorption spectra of all the compounds. The frontier orbitals of the complexes were influenced by the pattern of substitution, as can be seen in Figure 8, where the relative energies of orbitals between

Full Paper
doi.org/10.1002/ejic.202000423

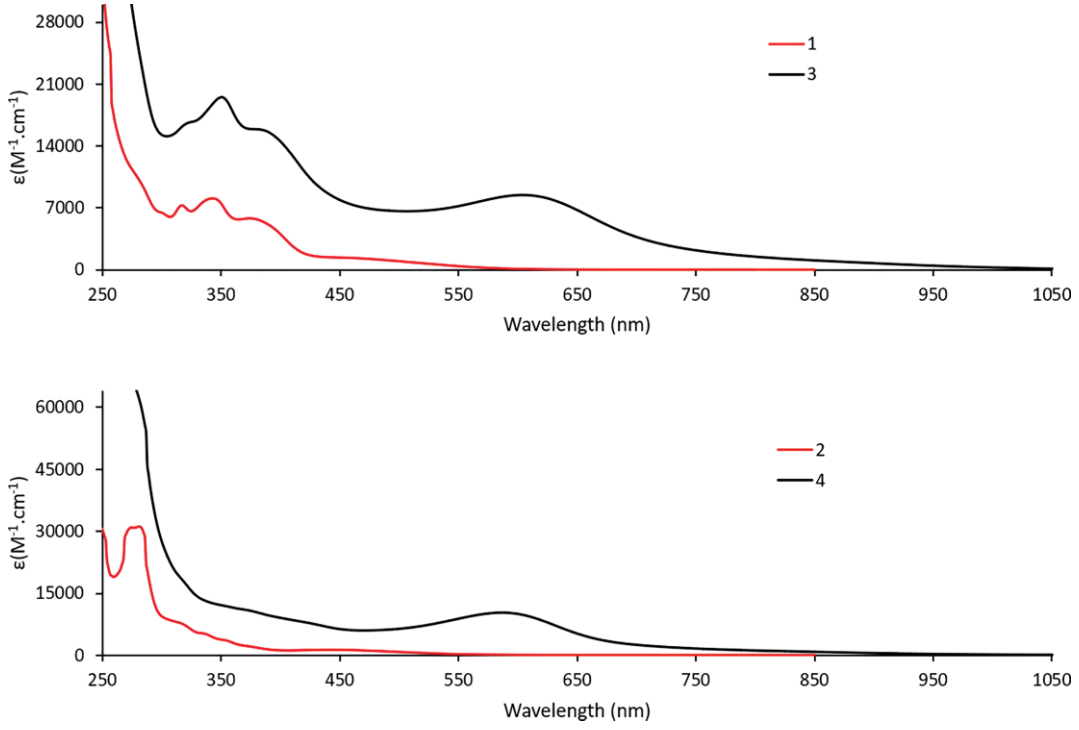

Figure 7. UV/Vis spectra of compounds **1**, **3**, **2** and **4** in $CHCl_3$.

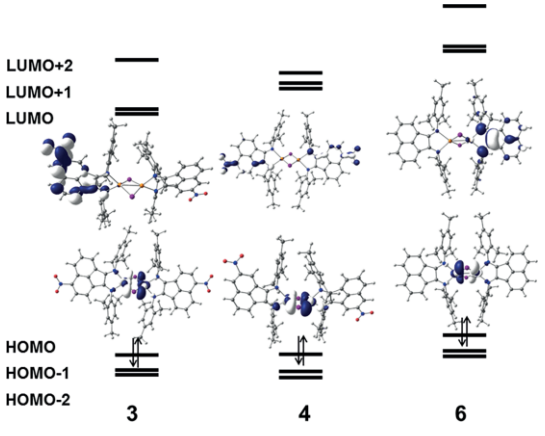

Figure 8. Frontier orbitals of complexes **3**, **4** and **6**, showing the 3D representation of the HOMO and the LUMO, as well as the relative energies.

HOMO-2 and LUMO+2 are shown, with a 3D representation of the HOMO and the LUMO.

In complex **6**, the HOMO is mainly localized in the $\{Cu_2(\mu\text{-}I)_2\}$ core, being antibonding between all atoms. There is a very small participation of the nitrogen lone pairs which are also Cu–N antibonding. The LUMO, on the other hand, is localized in the right side of the BIAN ligand. Note that the nitrogen atoms also participate in this π-system. The LUMO+1, not shown, looks the same, but is localized in the left side, and these two levels have practically the same energy (Figure 8).

The introduction of the NO_2 substituents leads to a stabilization of the LUMO, since the π-orbitals extend to the NO_2 groups, and this effect is more pronounced in **3** (*p*-NO_2). The effect on the HOMOs is not so significant and is very similar for **3** and **4**. The HOMO still consists of the σ network $[Cu_2(\mu\text{-}I)_2N_4]$ and remains antibonding. The main contribution of the unoccupied orbitals is from the π-orbitals ranging from the nitrogen atoms to the NO_2 groups over the whole ligand.

The TDDFT calculated lower energy absorption bands for the three complexes **3**, **4** and **6** are listed in Table S4 in SI, and all the orbitals are depicted in Figures S32, S33 and S34 in SI. The nature of the transitions is more clearly seen in the Electron Energy Difference Maps (EDDM) which are shown in Figure 9 and Figure 10 for complexes **3** and **4,** respectively. All the transitions are essentially metal-to-ligand-charge-transfer (MLCT) from orbitals including the $\{Cu_2(\mu\text{-}I)_2\}$ cores augmented by the nitrogen lone pairs (σ), represented in red in all figures to the ligand π-orbitals, represented in light blue. The participation of the nitrogen atoms in occupied (σ, n) and unoccupied (π*) orbitals adds to the essentially MLCT transitions an n→π* character (intra ligand, IL). The nature of the $\{Cu_2(\mu\text{-}I)_2\}$ σ and the ligand π* change with the transition. As the energy increases, the $\{Cu_2(\mu\text{-}I)_2\}$ σ orbitals will become more stable and less antibonding, the opposite being observed for the ligand π* orbitals (higher energy, more antibonding) as is shown in the molecular orbitals of the three complexes in Figures S32, S33 and S34 in SI.

The EDDM plots show that the low energy transitions involve the $\{Cu_2(\mu\text{-}I)_2\}$ cores and the ligands, but as the energy increases

Full Paper
doi.org/10.1002/ejic.202000423

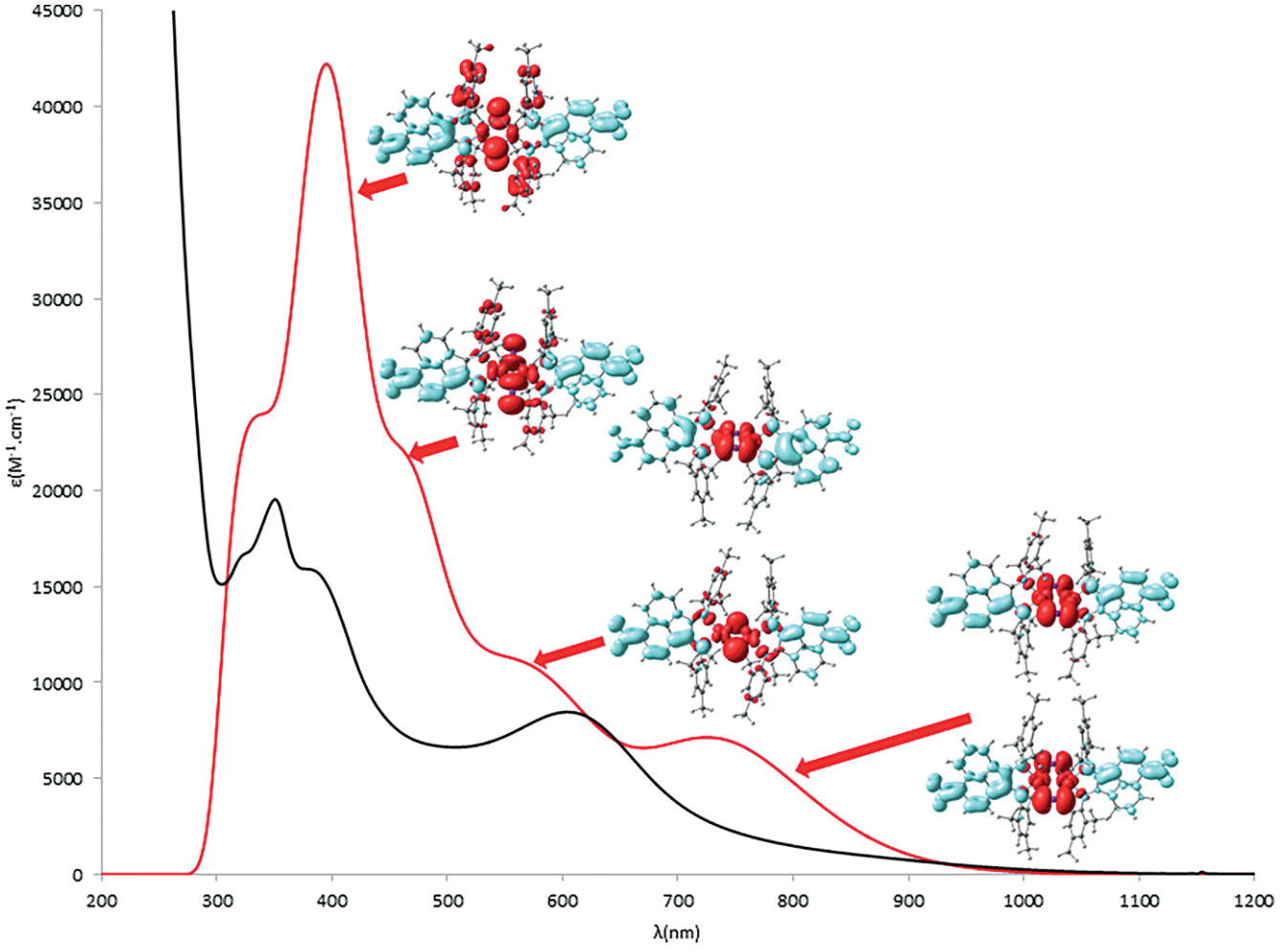

Figure 9. TDDFT simulated electronic spectrum of complex **3** (red) and experimental spectrum (black). The EDDM plots are also shown, red and blue corresponding to a decrease and increase in electron density, respectively.

(entries 5 and 6, Table S4) the participation of the phenyl substituents increases, adding a π→π* character (intra ligand, IL). The calculated spectra are shifted relative to the experimental ones, but their outline is very comparable.

The same type of plot is shown in Figure 10 for complex **4**. The EDDM plots are very similar to those of complex **3**, showing MLCT transitions, with some n→π* character (intra ligand, IL) in the lower energy bands, with added π→π* character (intra ligand, IL) in the higher energy bands.

The spectra of complex **6** are shown in Figure S35 in SI and display the same features, being mostly MLCT with added n→π* character. As expected, the π orbitals extension is smaller, owing to the absence of NO_2 substituents. On the other hand, the participation of phenyl contribution to the orbitals remains very reduced compared to what was observed for **3** and **4** in similar energy range, so that IL π→π* is practically non-existent.

In order to study the possible emission, complexes **3**, **4** and **6** were excited in the lower lying bands (620–630 nm) and also in higher lying bands (330–350 nm), but no steady state emission was observed. All complexes appear not to be luminescent in solution neither in solid phase.

Conclusions

Two dimeric new Cu(I) complexes $[Cu_2(\mu\text{-}I)_2(LL)_2]$ of two new bis(aryl-imino)-acenaphthene (LL), Ar-BIAN (Ar = 2,4,6-trimethylphenyl = mes) ligands, bearing the NO_2 group in the naphthalene moiety of the iminoacenaphthene at *para*- (**3**) and *meta*- (**4**) position were synthesized. Despite the similarities, the single-crystal X-ray diffraction structures showed that the $\{Cu_2(\mu\text{-}I)_2\}$ cores displayed different arrangements, being planar for **3** and puckered for **4**. Although it was possible to reproduce the main features of the geometries of these complexes using a DFT approach (and adding Grimme3 corrections to the functional), the fact that the analogous complexes with unsubstituted Ar-BIAN ligands also showed the same isomerism, led us to propose that packing effects should play a relevant role in determining the molecular structure. Indeed, the arrangement of the Ar groups is similar between the two puckered and the two planar complexes but differs between the two groups.

The nature of the TDDFT calculated absorption spectra in the visible is MLCT, in agreement with the experimental behaviour, but there is a n→π* character, resulting from transitions involving the N atoms lone pairs and their p orbitals present in

Full Paper
doi.org/10.1002/ejic.202000423

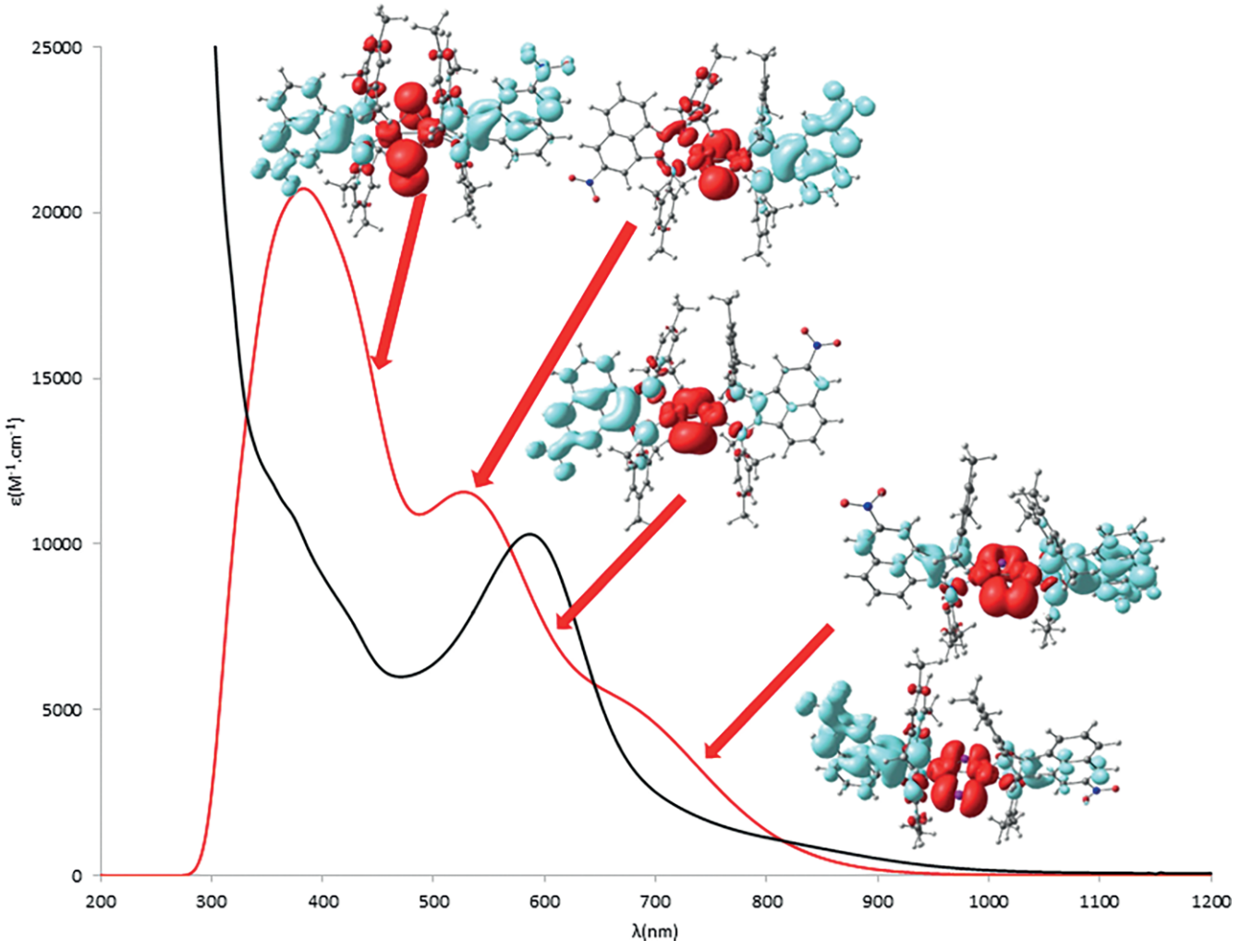

Figure 10. TDDFT simulated electronic spectrum of complex **4** (red) and experimental spectrum (black). The EDDM plots are also shown, red and blue corresponding to a decrease and increase in electron density, respectively.

the BIAN π orbitals. At higher energies the π orbitals of the Ar-groups also participate in the excitations.

Experimental Section

General: All manipulations dealing with air- or moisture-sensitive materials were carried out under an inert atmosphere using a dual vacuum/Argon line and standard Schlenk techniques. Unless otherwise stated, all reagents were purchased from commercial suppliers and used as received. All solvents were used under an inert atmosphere and purified prior to use. Dichloromethane and acetonitrile were purified over calcium hydride and distilled prior to use. Ligands Ar-BIAN (Ar = 2,4,6-trimethylphenyl) (**5**) and complex **6** were prepared according to the literature.[8,26]

Synthesis of nitro-Acenaphthenequinone: It was prepared following a slightly modified reported procedure.[38] Acenaphthenequinone was dissolved in concentrated H_2SO_4 (95–97 %) and after formation of a dark brown viscous solution the flask was placed in an ice-bath. The necessary amount of grinded $NaNO_3$ was then added slowly. The mixture was stirred during 3 h and then poured on crunched ice. The product was filtered and washed with cold water affording a 2:1 mixture of *para*/*meta* nitro-acenaphthenequinone. ^{1}H-NMR (400 MHz, $CDCl_3$, 25 °C) δ = 9.27 (s, 1H), 9.16 (d, J = 8 Hz, 2 H), 8.87 (s, 1H), 8.75 (d, J = 8 Hz, 2H), 8.53 (d, J = 8 Hz, 1H), 8.35–8.31 (m, 3H), 8.23 (d, J = 8 Hz, 2H), 8.16 (t, J = 8 Hz, 2H), 8.07 (t, J = 8 Hz, 1H) ppm.

Synthesis of Ligands 1 and 2: To a suspension of nitro-Acenaphthenequinone (1.14 g, 5.02 mmol) in ethanol, 2 equiv. of 2,4,6-methylaniline (1.44 mL, 10.04 mmol) were added together with 0.5 mL of formic acid. The mixture was stirred at R.T. overnight. A dark red solid precipitated, and it was separated from the solution by filtration affording 1.28 g (83 % yield) of **1**. The solvent of the remaining red solution was evaporated until dryness affording a red oil which was redissolved in CH_2Cl_2 (15 mL) and washed with HCl 0.1 M (4 × 5 mL) in order to remove the unreacted free aniline. The organic phase was separated, and the solvent removed under vacuum, yielding 0.60 g of a red solid, ligand **2** (78 % yield). Crystals of **1** were obtained by slow diffusion of hexane in a CH_2Cl_2 solution. Crystals of **2** were obtained by slow evaporation of an Et_2O solution.

Characterization of Ligand 1: Elemental analysis for $C_{30}H_{27}N_3O_2$·1/12CH_2Cl_2 calculated: C, 77.10; H, 5.84; N, 8.97; found C, 77.12; H, 5.90; N, 9.22. FTIR (ATR) ν = 1671 (C=N), 1638 (C=N), 1524 (N-O sym), 1329 (N-O asym) cm^{-1}. ^{1}H-NMR (400 MHz, $CDCl_3$) δ = 8.76 (d, J = 8 Hz, 1H), 8.31 (d, J = 8 Hz, 1H), 7.66 (t, J = 8 Hz, 1H), 6.99 (s, 4H), 6.94 (d, J = 8 Hz, 1H), 6.83 (d, J = 8 Hz, 1H), 2.39 (s, 6H), 2.08

(s, 12H) ppm. $^{13}C\{^1H\}$-NMR (100.6 MHz, $CDCl_3$) δ = 159.74, 159.53, 146.36, 145.22, 141.36, 134.72, 133.86, 133.53, 132.05, 130.05, 129.37, 129.30, 128.29, 127.10, 126.39, 124.37, 124.25, 124.05, 121.25, 21.04, 17.81 ppm. UV/Vis, λ_{max}[nm] (ε [L/(mol cm)]): 454(1338), 376(5773), 345(8013), 316(7200), 300(6439). ESI-MS: *m/z* = 462.1(100 %) [**1** + H]$^+$, 484.1(5 %) [**1** + Na]$^+$.

Characterization of Ligand 2: Elemental analysis for $C_{30}H_{27}N_3O_2 \cdot 1/5(CH_3CH_2)_2O$ calculated: C, 77.65; H, 6.14; N, 8.82; found C, 77.65; H, 5.98; N, 8.94. FTIR (ATR) ν = 1668 (C=N), 1635 (C=N), 1532 (N-O sym), 1338 (N-O asym) cm^{-1}. ^{1}H-NMR (400 MHz, $CDCl_3$) δ = 8.86 (s, 1H), 8.09 (d, *J* = 8 Hz, 1H), 7.57 (t, *J* = 8 Hz, 1H), 7.39 (s, 1H), 7.04 (s, 2H), 6.99 (s, 2H), 6.95 (d, *J* = 8 Hz, 1H), 2.41 (s, 3H), 2.38 (s, 3H), 2.09 (s, 12H) ppm. $^{13}C\{^1H\}$-NMR (100.6 MHz, $CDCl_3$) δ = 159.99, 159.82, 147.76, 146.42, 146.26, 142.08, 134.10, 133.52, 130.85, 130.51, 130.03, 129.81, 129.45, 129.28, 128.28, 126.03, 125.36, 124.47, 124.21, 116.40, 21.04, 21.01, 17.81 ppm. UV/Vis, λ_{max}[nm] (ε [L/(mol cm)]): 450(1251), 370(2253), 353(3617), 336(5191), 315(7840), 302(9056), 282(31128), 272(30435). ESI-MS: *m/z* = 462.1(100 %) [**2** + H]$^+$, 484.1(10 %) [**2** + Na]$^+$.

Synthesis of Complexes: To a CH_3CN (20 mL) solution of ligand **1** (137.60 mg, 0.30 mmol) or **2**, ((207.40 mg, 0.45 mmol) one equivalent of CuI was added, and the mixture was heated at reflux for 3 h. After removal of the solvent under vacuum, the resultant dark solid was washed with pentane (3 × 15 mL) and dried under vacuum. Suitable crystals for single-crystal X-ray structure determination were obtained by slow diffusion of pentane in a CH_2Cl_2 solution (yield **3**: 66 %, **4**: 59 % after crystallization).

Characterization of Complex 3: Elemental analyses for $C_{60}H_{54}Cu_2I_2N_6O_4 \cdot 1/6CH_2Cl_2$ calculated: C, 54.82; H, 4.15; N, 6.38; found C, 54.82; H, 4.20; N, 6.43. FTIR(ATR) ν = 1643 (C=N), 1530 (N-O sym), 1331 (N-O asym) cm^{-1}. ^{1}H-NMR (400 MHz, $CDCl_3$) δ = 8.76 (d, *J* = 8 Hz, 2H), 8.28 (d, *J* = 8 Hz, 2H), 7.65 (t, *J* = 8 Hz, 2H), 6.95 (s, 8H), 6.74 (d, *J* = 8 Hz, 2H), 6.65 (d, *J* = 8 Hz, 2H), 2.46 (s, 12H), 2.16 (s, 24H) ppm. $^{13}C\{^1H\}$-NMR (100.6 MHz, $CDCl_3$) δ = 160.49, 159.85, 145.46, 144.06, 143.99, 141.88, 134.89, 134.62, 133.94, 132.41, 129.69, 129.64, 129.00, 127.34, 127.29, 127.12, 124.61, 123.88, 121.75, 21.29, 19.29 ppm. UV/Vis, λ_{max}[nm] (ε [L/(mol cm)]): 820(1310), 610(8443), 380(15916), 351(19549), 318(16295). ESI-MS: *m/z* = 462.1(100 %) [**1** + H]$^+$, 985.0 (25 %) [2 × **1** + Cu]$^+$, 1174.8 (0.6 %) [**3**-I]$^+$.

Characterization of Complex 4: Elemental analyses for $C_{60}H_{54}Cu_2I_2N_6O_4 \cdot 1/3C_5H_{12}$ calculated: C, 55.77; H, 4.44; N, 6.33; found C, 56.03; H, 4.09; N, 6.44. FTIR(ATR) ν = 1649 (C=N), 1647 (C=N), 1536 (N-O sym), 1339 (N-O asym) cm^{-1}. ^{1}H-NMR (400 MHz, $CDCl_3$) δ = 8.88 (s, 2H), 8.13 (d, *J* = 8 Hz, 2H), 7.55 (t, *J* = 8 Hz, 2H), 7.21 (s, 2H), 6.93 (s, 4H), 6.86 (s, 4H), 6.79 (d, *J* = 8 Hz, 2H), 2.44 (s, 6H), 2.36 (s, 6H), 2.18 (s, 12H), 2.16 (s, 12H) ppm. $^{13}C\{^1H\}$-NMR (100.6 MHz, $CDCl_3$) δ = 160.59, 160.46, 148.03, 144.05, 143.95, 142.59, 135.07, 134.54, 131.67, 130.92, 129.84, 129.71, 129.62, 129.51, 128.86, 127.33, 127.07, 126.52, 126.05, 116.83, 21.22, 19.36, 19.30 ppm. UV/Vis, λ_{max}[nm] (ε [L/(mol.cm)]): 850(819), 586(10304), 372(10931), 353(11957), 317(18401), 304(24575) ESI-MS: *m/z* = 462.1(100 %) [**2** + H]$^+$, 985.0 (25 %) [2 × **2** + Cu]$^+$, 1174.8 (0.5 %) [**3**-I]$^+$.

Crystallographic Data: Crystals of **1**, **2**, **3** and **4** suitable for single-crystal X-ray analysis were grown as described in the synthetic procedures. Selected crystals were covered with Fomblin (polyfluoroether oil) and mounted on a nylon loop. The data were collected at 110(2) K on a Bruker D8 Venture diffractometer equipped with a Photon 100 CMOS detector and an Oxford Cryosystems gaseous nitrogen stream Cooler, using graphite monochromated Mo-K_α radiation (λ = 0.71073 Å). Data were processed using APEX2 suite software package, which includes integration and scaling (SAINT), absorption corrections (SADABS) and space group determination (XPREP). Structure solution and refinement were done using direct methods with the programs SHELXS-97 and SHEXL-2014/7 inbuilt in APEX and WinGX-Version 2014.1[53] software packages. All non-hydrogen atoms were refined anisotropically and all the hydrogen atoms were inserted in idealized positions and allowed to refine riding on the parent carbon atom. The crystals of **3** and **4** presented disordered solvent molecules and the PLATON/SQUEEZE[54] routine was applied as it was not possible to obtain a good disorder model. The crystals had poor diffracting power leading to poor quality data. The molecular diagrams were drawn with ORTEP-3 for Windows[55] and Mercury,[56] included in the software package. Table S5 contains crystallographic experimental data and structure refinement parameters.

Deposition Numbers 1979445–1979448 contain the supplementary crystallographic data for this paper. These data are provided free of charge by the joint Cambridge Crystallographic Data Centre and Fachinformationszentrum Karlsruhe Access Structures service www.ccdc.cam.ac.uk/structures.

Computational Studies: DFT calculations were performed with Gaussian16,[51] using the double-ζ basis set augmented with an *f* polarization function, LANL2DZ, for copper and extra *p* and *d* polarization function for iodine, with the associated effective core potential (ECP),[57] all downloaded from the EMSL Basis Set Library.[58,59] For the remaining elements, the standard 6-31G** basis set, comprising polarization functions, was employed. The hybrid PBE1PBE functional (also known as PBE0),[60] was used with a Grimme D3 dispersion correction.[61] The dispersion correction was necessary to reproduce relatively well the experimental structures, which were taken as starting geometry guesses. Geometry optimizations were performed without symmetry constraints in chloroform with the PCM solvation method.[62] TDDFT calculations, as implemented in Gaussian16, were performed to calculate the absorption spectra in chloroform. Wiberg indices were calculated with the NBO implementation in Gaussian16.[63–66] The reference compound with a non-supported Cu–Cu bond[67] was retrieved from the CSD.[52]

The electron density difference maps (EDDMs) were obtained from scripts in the GaussSum package.[68] Molecular structures orbitals and electron density were drawn using Chemcraft.[69]

ASSOCIATED CONTENT

Supporting Information (see footnote on the first page of this article): CCDC reference numbers 1979445–1979448. NMR spectra for all compounds (Fig. S1–S24). Mercury packing diagrams of **1** and **2** (Fig. S25) and **3** and **4** (Fig. S27). Molecular Structure of **6** (Fig. S26). Selected bond lengths and angles for **1**, **2** and **5** (Table S1) and for **3**, **4** and **6** (Table S2). Crystal data and structure refinement for **1**, **2**, **3** and **4** (Table S5). Optimized geometry of ligands **1** and **2** in the three possible conformations (Fig. S28). UV/Vis spectra of **5** and **6** (Fig. S31). Maxima and shoulders in the visible and near-UV absorption spectra of the ligands **1**, **2** and **5** and complexes **3**, **4**, and **6** in chloroform (Table S3). DFT calculated change in energy associated with lengthening the Cu–Cu distance from 2.566 to 3.071 Å in complex **3** (Fig. S29). The X-ray structure of a complex with a non-supported Cu(I)–Cu(I) bond (top) and a view of the ligand (bottom) (Fig. S30). TDDFT calculated excitation energies and oscillator strengths (OS) in the visible absorption spectra of the complexes **3**, **4**, and **6** in chloroform (Table S4). Frontier molecular orbitals of complexes **3**, **4** and **6** (Fig. S32–S34). TDDFT simulated

electronic spectrum, experimental spectrum and EDDM plot of complex **6**, (Figure S35).

Author Information

Conflicts of interest

There are no conflicts of interest to declare.

Acknowledgments

This work was supported by the Associate Laboratory for Green Chemistry- LAQV financed by national funds from FCT/MCTES (UIDB/50006/2020). M. J. C. and M. O. acknowledge the Fundação para a Ciência e a Tecnologia (FCT) for support (UIDB/04046/2020 and UIDP/04046/2020). The authors acknowledge LabRMN at FCT-UNL and Rede Nacional de RMN (RNRMN) for access to the facilities. The NMR spectrometers are part of The National NMR Facility, supported by FCT (ROTEIRO/0031/2013 - PINFRA/22161/2016) (co-financed by FEDER through COMPETE 2020, POCI, and PORL and FCT through PIDDAC). Data Mass Spectrometry obtained by the Laboratório de Análises/LAQV REQUIMTE - Chemistry department FCT University NOVA of Lisbon. The SCXR determinations were performed in house (equipment financed by national funds through project RECI/BBB-BEP/0124/2012 from FCT/MCTES). S. B. acknowledges project SmartBioR for financial support (CENTRO-01–0145-FEDER-000018, Integrated Programme SR&TD co-funded by Centro 2020 program, Portugal 2020, European Union, through the European Regional Development Fund). M. O. acknowledges PhD Grant SFRH/BD/120985/2016 financed by FCT.

Keywords: Copper(I) · Functionalized Ar-BIAN · Synthesis · Density Function Calculations · Crystal Structure

[1] P. J. Pérez, M. M. Díaz-Requejo, in *Compr. Organomet. Chem. III* (Eds.: R. H. Crabtree, D. M. P. Mingos), Elsevier, New York, **2007**, pp. 153–195.
[2] V. W.-W. Yam, K. K.-W. Lo, *Chem. Soc. Rev.* **1999**, *28*, 323–334.
[3] M. W. Blaskie, D. R. McMillin, *Inorg. Chem.* **1980**, *19*, 3519–3522.
[4] K. Tsuge, Y. Chishina, H. Hashiguchi, Y. Sasaki, M. Kato, S. Ishizaka, N. Kitamura, *Coord. Chem. Rev.* **2016**, *306*, 636–651.
[5] S. K. Gibbons, R. P. Hughes, D. S. Glueck, A. T. Royappa, A. L. Rheingold, R. B. Arthur, A. D. Nicholas, H. H. Patterson, *Inorg. Chem.* **2017**, *56*, 12809–12820.
[6] H. tom Dieck, M. Svoboda, T. Greiser, *Z. Naturforsch. B* **1981**, *36*, 823–832.
[7] G. Van Koten, K. Vrieze, in *Adv. Organomet. Chem.* **1982**, pp. 151–239.
[8] R. van Asselt, C. J. Elsevier, W. J. J. Smeets, A. L. Spek, R. Benedix, *Rec. Trav. Chim. Pays-Bas* **2010**, *113*, 88–98.
[9] B. Rieger, L. S. Baugh, S. Kacker, S. Striegler, *Late Transition Metal Polymerization Catalysis*, Wiley-VCH Verlag, Weinheim, **2006**.
[10] S. D. Ittel, L. K. Johnson, M. Brookhart, *Chem. Rev.* **2000**, *100*, 1169–1203.
[11] V. C. Gibson, S. K. Spitzmesser, *Chem. Rev.* **2003**, *103*, 283–315.
[12] G. J. P. Britovsek, V. C. Gibson, D. F. Wass, *Angew. Chem. Int. Ed.* **1999**, *38*, 428–447.
[13] J. H. Groen, J. G. P. Delis, P. W. N. M. van Leeuwen, K. Vrieze, *Organometallics* **1997**, *16*, 68–77.
[14] J. Durand, B. Milani, *Coord. Chem. Rev.* **2006**, *250*, 542–560.
[15] A. Scarel, M. R. Axet, F. Amoroso, F. Ragaini, C. J. Elsevier, A. Holuigue, C. Carfagna, L. Mosca, B. Milani, *Organometallics* **2008**, *27*, 1486–1494.
[16] B. L. Small, R. Rios, E. R. Fernandez, M. J. Carney, *Organometallics* **2007**, *26*, 1744–1749.
[17] V. Rosa, P. J. Gonzalez, T. Avilés, P. T. Gomes, R. Welter, A. C. Rizzi, M. C. G. Passeggi, C. D. Brondino, *Eur. J. Inorg. Chem.* **2006**, *2006*, 4761–4769.
[18] V. Rosa, T. Avilés, G. Aullon, B. Covelo, C. Lodeiro, *Inorg. Chem.* **2008**, *47*, 7734–7744.
[19] V. Rosa, C. I. M. Santos, R. Welter, G. Aullón, C. Lodeiro, T. Avilés, *Inorg. Chem.* **2010**, *49*, 8699–8708.
[20] T. Kauf, V. Rosa, C. Fliedel, R. Pattacini, N. Deibel, T. Avilés, B. Sarkar, P. Braunstein, *Dalton Trans.* **2015**, *44*, 5441–5450.
[21] B. Pedras, V. Rosa, R. Welter, C. Lodeiro, T. Avilés, *Inorg. Chim. Acta* **2012**, *381*, 143–149.
[22] V. Rosa, S. A. Carabineiro, T. Avilés, P. T. Gomes, R. Welter, J. M. Campos, M. R. R. M. R. Ribeiro, *J. Organomet. Chem.* **2008**, *693*, 769–775.
[23] C. Romain, V. Rosa, C. Fliedel, F. Bier, F. Hild, R. Welter, S. Dagorne, T. Avilés, *Dalton Trans.* **2012**, *41*, 3377–3379.
[24] C. Fliedel, V. Rosa, C. I. M. Santos, P. J. Gonzalez, R. M. Almeida, C. S. B. Gomes, P. T. Gomes, M. A. N. D. A. Lemos, G. Aullón, R. Welter, T. Avilés, *Dalton Trans.* **2014**, *43*, 13041–13054.
[25] L. Li, P. S. Lopes, V. Rosa, C. A. Figueira, M. A. N. D. A. Lemos, M. T. Duarte, T. Avilés, P. T. Gomes, *Dalton Trans.* **2012**, *41*, 5144–5154.
[26] L. Li, P. S. Lopes, C. A. Figueira, C. S. B. Gomes, M. T. Duarte, V. Rosa, C. Fliedel, T. Avilés, P. T. Gomes, *Eur. J. Inorg. Chem.* **2013**, *2013*, 1404–1417.
[27] P. De Frémont, H. Clavier, V. Rosa, T. Avilés, P. Braunstein, *Organometallics* **2011**, *30*, 2241–2251.
[28] T. Kern, U. Monkowius, M. Zabel, G. Knör, *Eur. J. Inorg. Chem.* **2010**, *2010*, 4148–4156.
[29] T. Kern, U. Monkowius, M. Zabel, G. Knör, *Inorg. Chim. Acta* **2011**, *374*, 632–636.
[30] C. J. Adams, N. Fey, J. A. Weinstein, *Inorg. Chem.* **2006**, *45*, 6105–6107.
[31] C. J. Adams, N. Fey, Z. A. Harrison, I. V. Sazanovich, M. Towrie, J. A. Weinstein, *Inorg. Chem.* **2008**, *47*, 8242–8257.
[32] S. K. Singh, S. K. Dubey, R. Pandey, L. Mishra, R.-Q. Zou, Q. Xu, D. S. Pandey, *Polyhedron* **2008**, *27*, 2877–2882.
[33] D. A. Evans, L. M. Lee, I. Vargas-Baca, A. H. Cowley, *Dalton Trans.* **2015**, *44*, 11984–11996.
[34] D. A. Evans, L. M. Lee, I. Vargas-Baca, A. H. Cowley, *Organometallics* **2015**, *34*, 2422–2428.
[35] P. A. Papanikolaou, N. V. Tkachenko, *Phys. Chem. Chem. Phys.* **2013**, *15*, 13128–13136.
[36] J. W. Kee, Y. Y. Ng, S. A. Kulkarni, S. K. Muduli, K. Xu, R. Ganguly, Y. Lu, H. Hirao, H. S. Soo, *Inorg. Chem. Front.* **2016**, *3*, 651–662.
[37] Y. Y. Ng, L. J. Tan, S. M. Ng, Y. T. Chai, R. Ganguly, Y. Du, E. K. L. Yeow, H. Sen Soo, *ACS Catal.* **2018**, *8*, 11277–11286.
[38] L. Wang, X. Wang, J. Cui, W. Ren, N. Meng, J. Wang, X. Qian, *Tetrahedron: Asymmetry* **2010**, *21*, 825–830.
[39] Y. Xiao, X. Qian, *Tetrahedron Lett.* **2003**, *44*, 2087–2091.
[40] H. A. Jenkins, C. L. Dumaresque, D. Vidovic, J. A. C. Clyburne, *Can. J. Chem.* **2002**, *80*, 1398–1403.
[41] U. El-Ayaan, F. Murata, S. El-Derby, Y. Fukuda, *J. Mol. Struct.* **2004**, *692*, 209–216.
[42] M. Gasperini, F. Ragaini, E. Gazzola, A. Caselli, P. Macchi, *Dalton Trans.* **2004**, 3376–3382.
[43] J. A. Moore, K. Vasudevan, N. J. Hill, G. Reeske, A. H. Cowley, *Chem. Commun.* **2006**, 2913–2915.
[44] U. El-Ayaan, A. Paulovicova, Y. Fukuda, *J. Mol. Struct.* **2003**, *645*, 205–212.
[45] D. N. Coventry, A. S. Batsanov, A. E. Goeta, J. A. K. Howard, T. B. Marder, *Polyhedron* **2004**, *23*, 2789–2795.
[46] L. Li, C. S. B. Gomes, P. T. Gomes, M. T. Duarte, Z. Fan, *Dalton Trans.* **2011**, *40*, 3365–3380.
[47] H. D. De Ahna, H. D. Hardt, *Z. Anorg. Allg. Chem.* **1972**, *387*, 61–71.
[48] J. K. Cheng, Y. G. Yao, J. Zhang, Z. J. Li, Z. W. Cai, X. Y. Zhang, Z. N. Chen, Y. B. Chen, Y. Kang, Y. Y. Qin, et al., *J. Am. Chem. Soc.* **2004**, *126*, 7796–7797.
[49] P. C. Healy, C. Pakawatchai, A. H. White, *J. Chem. Soc., Dalton Trans.* **1985**, 2531–2539.
[50] C. Näther, I. Jeß, N. Lehnert, D. Hinz-Hübner, *Solid State Sci.* **2003**, *5*, 1343–1357.
[51] M. J. Frisch, G. W. Trucks, H. B. Schlegel, G. E. Scuseria, M. A. Robb, J. R. Cheeseman, G. Scalmani, V. Barone, B. Mennucci, G. A. Petersson, H. Nakatsuji, M. Caricato, X. Li, H. P. Hratchian, A. F. Izmaylov, J. Bloino, G. Zheng, J. L. Sonnenberg, M. Hada, M. Ehara, K. Toyota, R. Fukuda, J. Hasegawa, M. Ishida, T. Nakajima, Y. Honda, O. Kitao, H. Nakai, T. Vreven, J. A. Montgomery Jr., J. E. Peralta, F. Ogliaro, M. Bearpark, J. J. Heyd, E. Broth-

ers, K. N. Kudin, V. N. Staroverov, R. Kobayashi, J. Normand, K. Raghavachari, A. Rendell, J. C. Burant, S. S. Iyengar, J. Tomasi, M. Cossi, N. Rega, J. M. Millam, M. Klene, J. E. Knox, J. B. Cross, V. Bakken, C. Adamo, J. Jaramillo, R. Gomperts, R. E. Stratmann, O. Yazyev, A. J. Austin, R. Cammi, C. Pomelli, J. W. Ochterski, R. L. Martin, K. Morokuma, V. G. Zakrzewski, G. A. Voth, P. Salvador, J. J. Dannenberg, S. Dapprich, A. D. Daniels, Ö. Farkas, J. B. Foresman, J. V. Ortiz, J. Cioslowski, D. J. Fox, *Gaussian 09, Revision C.01*, Gaussian, Inc., Wallingford CT, **2016**.

[52] C. R. Groom, I. J. Bruno, M. P. Lightfoot, S. C. Ward, *Acta Crystallogr., Sect. B Struct. Sci. Cryst. Eng. Mater.* **2016**, *72*, 171–179.

[53] L. J. Farrugia, *J. Appl. Crystallogr.* **2012**, *45*, 849–854.

[54] A. L. Spek, *Acta Crystallogr., Sect. C Struct. Chem.* **2015**, *71*, 9–18.

[55] L. J. Farrugia, *J. Appl. Crystallogr.* **1997**, *30*, 565.

[56] C. F. Macrae, P. R. Edgington, P. McCabe, E. Pidcock, G. P. Shields, R. Taylor, M. Towler, J. Van De Streek, *J. Appl. Crystallogr.* **2006**, *39*, 453–457.

[57] L. E. Roy, P. J. Hay, R. L. Martin, *J. Chem. Theory Comput.* **2008**, *4*, 1029–1031.

[58] D. Feller, *J. Comput. Chem.* **1996**, *17*, 1571–1586.

[59] K. L. Schuchardt, B. T. Didier, T. Elsethagen, L. Sun, V. Gurumoorthi, J. Chase, J. Li, T. L. Windus, *J. Chem. Inf. Model.* **2007**, *47*, 1045–1052.

[60] C. Adamo, V. Barone, *J. Chem. Phys.* **1999**, *110*, 6158–6170.

[61] S. Grimme, *J. Comput. Chem.* **2004**, *25*, 1463–1473.

[62] A. V. Marenich, C. J. Cramer, D. G. Truhlar, *J. Phys. Chem. B* **2009**, *113*, 6378–6396.

[63] A. E. Reed, R. B. Weinstock, F. Weinhold, *J. Chem. Phys.* **1985**, *83*, 735–746.

[64] J. P. Foster, F. Weinhold, *J. Am. Chem. Soc.* **1980**, *102*, 7211–7218.

[65] A. E. Reed, L. A. Curtiss, F. Weinhold, *Chem. Rev.* **1988**, *88*, 899–926.

[66] F. Weinhold, J. E. Carpenter, in *The Structure of Small Molecules and Ions*, (Eds.: R. Naaman, Z. Vager), Plenum, **1988**, pp. 227–236.

[67] M. Nishikawa, T. Sano, M. Washimi, K. Takao, T. Tsubomura, *Dalton Trans.* **2016**, *45*, 12127–12136.

[68] N. M. O'Boyle, A. L. Tenderholt, K. M. Langner, *J. Comput. Chem.* **2008**, *29*, 839–845.

[69] G. A. Zhurko, "Chemcraft - graphical software for visualization of quantum chemistry computations", http://www.chemcraftprog.com/index.html, **2013**; last accessed April **2020**.

Received: April 30, 2020